Oil Shale, 2021, Vol. 38, No. 4, pp. 317–337
doi: https://doi.org/10.3176/oil.2021.4.03

Numerical study of the flow, heat transfer and pyrolysis process in the gas full circulation oil shale retort

Luwei Pan[(a)], Hao Lu[(a)], Fangqin Dai[(a)]*, Shaohui Pei[(b,c)], Qicheng Wu[(b)], Jianning Huang[(b,c)]

Received 2 March 2021, accepted 10 November 2021, available online 10 December 2021

(a) The State Key Laboratory of Refractories and Metallurgy, Wuhan University of Science and Technology, No.947 Heping Avenue, Qingshan District, Wuhan 430081, P. R. China
(b) Liaoning Chengda Co. Ltd., No.71 Renmin Road, Zhongshan District, Dalian 116000, P. R. China
(c) Xinjiang BaoMing Mines Co. Ltd., No.21 Wenhua Road, Jimsar 831700, P. R. China

Abstract. *A three-dimensional mathematical model of the 300 t/d gas full circulation oil shale retort is developed to investigate the flow-thermo-pyrolysis behaviors in the retorting process in this work. The velocity of reheated recycled gas decreases gradually from the wall regions toward the central regions of the retort on the same horizontal surface, and the velocity of oil shale is just the opposite. In the pre-heating and retorting stages, the average temperature of gases is about 30 °C higher than that of oil shale on the same level, and the temperatures of gas and oil shale both decrease gradually from the wall regions to the three central regions, which results in that the pyrolysis reaction of oil shale gradually diffuses from the former regions to the latter regions during the downward-moving process. The results also illustrate that oil shale particles larger than 50 mm and smaller than 20 mm should be mixed with 20–50 mm oil shale particles at a proper ratio rather than being fed into the retort directly, to enhance oil yield and the thermal efficiency of the retort.*

Keywords: *gas full circulation oil shale retort, pyrolysis, heat transfer, mass transfer.*

* Corresponding author: e-mail *daifangqin@wust.edu.cn*

1. Introduction

The oil shale retorting, in which raw oil shale is thermally treated to convert it into shale oil and combustible gas, is regarded as a valuable supplemental industrial process of conventional oil manufacturing [1–5]. Over the past two decades, the oil shale retorting industry has seen substantial technological development. Several new technologies such as Alberta Taciuk process (ATP), Sanjiang (SJ) gas-combustion retorting process, Enefit-280 retort, Petroter retort and gas full circulation retort have been developed and commenced full commercial operation [6–8]. The operation situation of the world oil shale retorting industry is shown in Table 1.

Table 1. Operation situation of oil shale retorting in 2018 [6, 9]

Country	Retorting process	Heat carrier type	Capacity, t/d	Retort amount	Commencement of operation
China	Fushun-type	Gas	100	560	1930s
	SJ type	Gas	300	8	2010
	Gas full circulation type	Gas	300	64	2012
	ATP	Solids	6000	1	2016
Estonia	Kiviter	Gas	100	8	1950s
			200	49	1950s
			1000	2	1980s
	Enefit-140	Solids	3000	2	2003
	Enefit-280		6000	1	2012
	Petroter		3000	3	2010s
Brazil	Petrosix	Gas	2500	1	1981
			6000	1	1991

The choice of retort type depends not only on the economic, environmental and maturity implications of the retorting technology, but also on the characteristics of oil shale used [6]. For example, the SJ gas-combustion retorting technology can take full advantage of semi-coke and achieve the oil production rate higher than 90%, while exploiting Chinese Yaojie oil shale, which is of high oil yield (more than 11%) and high fixed carbon content (greater than 5.8%) [6]. However, the combustion of semi-coke can neither supply valuable and sufficient heat for oil shale pyrolysis nor direct extra air

into the retort, which massively increases the gas displacement and reduces the oil production rate and the combustive gas caloricity of the SJ retort, while retorting the oil shale from the southeastern margin of the Junggar Basin (China) of medium oil yield (about 7%), low fixed carbon content (about 3%) and high combustive gas yield [10].

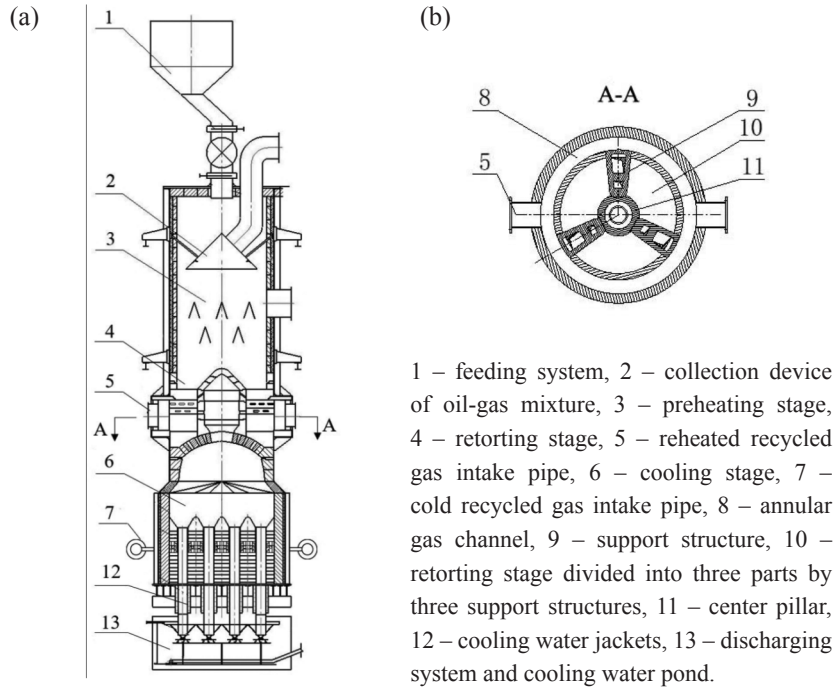

Fig. 1. The structure of the gas full circulation oil shale retort: (a) main view, (b) cross-sectional view (A–A).

Hence, the gas full circulation retort is developed to pyrolyze this oil shale in the current work. The retort includes a preheating stage, a retorting stage and a cooling stage. The retorting stage is divided into three parts by three support structures and the center pillar, as shown in Figure 1. In the retorting process, oil shale is firstly grinded and separated into different size ranges: 6–20 mm, 20–30 mm, 30–50 mm and 50–55 mm. The remaining detrital particles smaller than 10 mm are pressed into oil shale balls through a pelletizer. Then those particle groups are fed into the retort or fed into it after mixing at different proportions. Meanwhile, the reheated recycled gas is blown into the annular channel from the gas intake pipe and then into the retort via the orifices in the wall of the retorting stage and the support structures to supply heat for the retorting reaction, and the cold recycled gas is blown into the retort from the bottom to make full use of the heat of semi-coke.

Oil shale is heated in the pre-heating and retorting stages with the recycled gas during the gradually yet continuously downward-flowing process, and is converted into semi-coke and the oil-gas mixture completely in the retorting stage. Semi-coke is cooled to about 370 °C by the cold recycled gas during flowing to the bottom of the cooling stage, then is cooled to environment temperature in the cooling water pond and pushed out by the pusher machine. Ultimately, this semi-coke with no combustion value is used to manufacture hollow bricks, cement and ceramsite. The oil-gas mixture flowing out from the top of the retort is separated to shale oil and gas by the cryogenic separator, the electrostatic oil separator and the water scrubbing tower. The separated gas is divided into three parts: reheated recycle gas, cold recycled gas and burning gas. The reheated recycle gas is recycled back to the retort after being heated by combusting the burning gas and outsourcing fuel gas through hot-blast stoves. The cold recycled gas is directly recycled back to the bottom of the retort to exchange heat with semi-coke.

The rules of oil shale and gas flows, heat transfer, pyrolysis reactions and mass transfer in the gas full circulation oil shale retort and other oil shale retorting technologies are difficult to understand because of their complexity. Operations and improvements of the oil shale retorts are mainly based on pilot-scale production and experience, without corresponding theoretical guidance. Therefore, the numerical analysis of the retorting process can be beneficial for retort design and operation improvement, which are responsible for heat exchange efficiency, products yield and oil quality [11–13].

However, to date, modeling studies about the flow-thermo-pyrolysis behaviors of the oil shale retorting process have been very few [14]. The primary reason is that the flow of oil shale particles and the multiple heat transfer processes in different stages cannot be described accurately. Unlike the coking process in the coke oven where coal is fixed in the regular shaped coking chamber, the oil shale retort usually consists of the pre-heating stage, the heating stage and the cooling stage or gasification stage with irregular shape, which results in that the flow and heat transfer characteristics are more complicated than those in the coke oven. Hence the flow and heat transfer model used in coke oven simulation cannot be applied to oil shale retort simulation. Besides, coupling a suitable pyrolysis model with the flow and heat transfer model is also difficult. Few kinetic models have been developed for the devolatilization of various oil shales. Even though some network pyrolysis models on oil shale pyrolysis have been reported, such as Functional-Group, Depolymerization, Vaporization, Cross-linking (FG-DVC) model, Continuing Professional Development (CPD) model, Flash Chain model, etc. [15–18], which are applicable to a wide range of oil shale types for rapid pyrolysis, they are extremely complex and difficult to use for the retorting process which is a slow devolatilization process [19].

The aim of this paper is to develop a three-dimensional mathematical model of the gas full circulation oil shale retort on the basis of the dual mesh method,

and investigate the characteristics of oil shale materials, as well as gas flows, heat transfer and pyrolysis reactions of the pyrolysis process in the retort. This work is expected to contribute to a better understanding of the retorting process, facilitating the optimization operation of the gas full circulation oil shale retort and providing a theoretical method for the numerical simulation of other oil shale retorting technologies.

2. Mathematical model

The height of the gas full circulation oil shale retort is 12 m, including the 4 m preheating stage (containing a 1.5 m storing stage), the 4.1 m retorting stage and the 3.9 m cooling stage. The dual mesh method is used to develop the 3-D mathematical model of the retort. As shown in Figure 2, the mathematical model of the retort consists of the oil shale flowing region and the gas flowing region, which are used to describe the oil shale materials flowing process and the gas flowing process, respectively. The corresponding grids of the two regions are identical and are associated through compiling programs to calculate the energy and mass transfer processes between oil shale and gas heat carrier.

To simplify the mathematical model, the following hypotheses were introduced: (1) The break of oil shale/semi-coke during the retorting process was ignored. (2) Oil shale was continuously flowing down from the bottom of the 1.5 m storing stage. (3) The cold recycled gas was uniformly blown into the retort from the bottom of the cooling stage. (4) The physical and chemical properties of the oil-gas mixture were identical to those of the recycled gas.

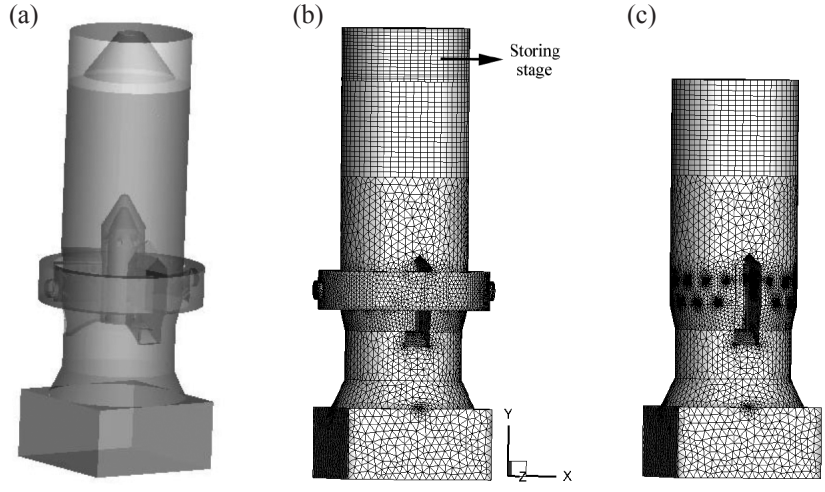

Fig. 2. The model of the gas full circulation oil shale retort (a), the grid partition of the gas flowing region (b), the oil shale flowing region (c).

2.1. Equations governing the oil shale flowing region

Equations governing the oil shale flowing region are the following:

(1) Continuity equation:

$$\frac{\partial(1-\varepsilon)\rho_{os}}{\partial t}+\nabla\cdot\left((1-\varepsilon)\rho_{os}\overrightarrow{v_{os}}\right)=-S_{mix}, \tag{1}$$

where ε represents the voidage of the oil shale packed bed, ρ_{os} is the oil shale density, $\overrightarrow{v_{os}}$ is the superficial velocity, S_{mix} is the formation rate of oil shale pyrolysis products.

(2) Momentum equation:

$$(1-\varepsilon)\rho_{os}\left[\frac{\partial\overrightarrow{v_{os}}}{\partial t}+\left(\overrightarrow{v_{os}}\cdot\nabla\right)\overrightarrow{v_{os}}\right]=(1-\varepsilon)\mu_{os}\nabla^2\overrightarrow{v_{os}}, \tag{2}$$

where μ_{os} is the dynamic viscosity of oil shale particles.

(3) Energy equation:

$$\begin{aligned}&(1-\varepsilon)\left(\rho c_p\right)_{os}\frac{\partial T_s}{\partial t}+\left(\rho c_p\right)_{os}\cdot\overrightarrow{v_{os}}\cdot\nabla T_{os}=\\&(1-\varepsilon)\nabla\left(\lambda_{os}\nabla T_{os}\right)+h_v(T_g-T_{os})+Q_{\mathrm{r}}+Q_{\mathrm{rs}}+Q_{\mathrm{p}}+Q_q,\end{aligned} \tag{3}$$

where T_{os} and T_g are the oil shale and gas temperature, respectively, $c_{p,os}$ and λ_{os} delegate the effective heat capacity and thermal conductivity of oil shale, respectively, Q_p is the heat of gaseous pyrolysis products, Q_{rs} is the heat of the pyrolysis reaction concentrating in the temperature range of 250–530 °C, Q_q is the vaporization latent heat of surface moisture, which is considered by introducing equivalent specific heat according to Jin et al. [20], Q_r represents the radiative heat transfer among oil shale particles. By using the Rosseland approximation [21], the radiative heat transfer can be defined as follows:

$$Q_r=\nabla q_r=\nabla\left(-k_r dT_{os}/dx\right)=\nabla\left[-\left(16\sigma n^2T_{os}^3/3\beta_e\right)dT_{os}/dx\right], \tag{4}$$

where σ is the Stefan-Boltzmann constant, n is the refractive index, k_r can be considered as the 'irradiative conductivity' [22] and β_e is the extinction coefficient of the oil shale packing bed [23] expressed as:

$$\beta_e=3(1-\varepsilon)/d_p, \tag{5}$$

where d_p is the average particle diameter of the oil shale particle group.

The volumetric convection heat transfer coefficient h_v can be calculated from the following equation:

$$h_v = h_{osf}\alpha_{osf}, \tag{6}$$

where h_{osf} represents the heat transfer coefficient between oil shale and recycled gas, and α_{osf} represents the specific surface area of per unit volume. According to literarure [23–25], the formulas of h_{osf} and α_{osf} can be expressed as:

$$h_{sf} = \frac{\left(2.0 + 1.1\mathrm{Pr}^{1/3}\,\mathrm{Re}^{0.6}\right)\lambda_g}{d_p}, \tag{7}$$

$$\alpha_{osf} = 6\left(1-\varepsilon\right)/d_p, \tag{8}$$

where $\mathrm{Pr} = (c_p\mu)_g / \lambda_g$ is the Prandtl number of gas and $\mathrm{Re} = \varepsilon\rho_g d_p v_g / \mu_g$ is the Reynolds number of gas.

2.2. Equations governing the gas flowing region

Equations governing the gas flowing region include the following:

(1) Continuity equation:

$$\frac{\partial\varepsilon\rho_g}{\partial t} + \nabla\cdot\left(\varepsilon\rho_g\overrightarrow{v_g}\right) = S_{mix}, \tag{9}$$

where ρ_{os} is the density of recycled gas.

(2) Momentum equation:

$$\varepsilon\rho_g\left[\frac{\partial\overrightarrow{v_g}}{\partial t} + \left(\overrightarrow{v_g}\cdot\nabla\right)\overrightarrow{v_g}\right] = -\varepsilon\nabla p + \varepsilon\mu_g\nabla^2\overrightarrow{v_g} - \overline{S}, \tag{10}$$

where p is the pressure, $\overline{S}$ is the momentum source term of gas through the oil shale/semi-coke bed:

$$\overline{S} = -\left(\frac{\mu}{\mathrm{a}}\overrightarrow{v_g} + C_2\frac{1}{2}\rho u_{mag}\overrightarrow{v_g}\right). \tag{11}$$

The Ergun and Blake-Kozeny equations are used to calculate the viscous resistance coefficient 1/a and inertial resistance coefficient C_2 of the oil shale bed [26]:

$$\frac{1}{\mathrm{a}} = \frac{160}{d_p^2}\frac{(1-\varepsilon)^2}{\varepsilon^3}, \tag{12}$$

$$C_2 = \frac{1.61}{d_p}\frac{(1-\varepsilon)}{\varepsilon^3}. \tag{13}$$

(3) Energy equation:

$$\varepsilon\left(\rho c_p\right)_g \frac{\partial T_g}{\partial t} + \left(\rho c_p\right)_g \cdot \overrightarrow{v_g} \cdot \nabla T_g = \nabla \cdot \left[\varepsilon\lambda_g \nabla T_g - \left(\sum_i h_i J_i\right) + \left(\overline{\overline{\tau}} \cdot \overrightarrow{v_g}\right)\right] + h_v (T_{os} - T_g) + Q_p, \tag{14}$$

where $c_{p,g}$ and λ_g delegate the effective heat capacity and thermal conductivity of recycled gas, respectively.

2.3. Oil shale pyrolysis model

Oil shale pyrolysis is a complex reaction scheme, any set of parameters cannot be expected to represent kinetic data accurately over a wide range of conditions. Popular coal pyrolysis models are network pyrolysis models, but these models are valid in a rapid oil shale pyrolysis and are difficult to use in a slow oil shale pyrolysis. To simulate the oil shale pyrolysis process, the gaseous pyrolysis products (the oil-gas mixture) are regarded as one component, and the mixture's physical and chemical properties are identical to those of the recycled gas.

The kinetic equation of the pyrolysis products generation is [27]:

$$\frac{dm}{dT} = \frac{Am_f}{\beta}\exp\left[-\frac{E}{RT} - \frac{ART^2}{\beta E}\exp\left(-\frac{E}{RT}\right)\cdot\left(1 + \frac{2!}{E/RT} + \frac{3!}{(E/RT)^2} + \ldots\right)\right], \tag{15}$$

where m_T is the production of pyrolysis products at temperature T, m_f is the total production of pyrolysis products, A is the pre-exponential factor, E is the apparent activation energy, R is the ideal gas constant, T is the absolute temperature, t is the heating time, β is the heating rate of pyrolysis process, α is the conversion rate of oil shale, w_o the initial mass of oil shale, w_T is the oil shale mass at temperature T, w_f is the oil shale mass after pyrolysis reaction.

The pyrolysis characteristics of oil shale from the southeastern margin of the Junggar Basin at different heating rates have been investigated through thermogravimetric analysis (TGA) [28, 29]. According to these data, the pre-exponential factor and the apparent activation energy were calculated in the current work:

$$A = 3.4e^{+17}s^{-1}, \quad E = 280 \text{ kJ/mol}.$$

3. Results and discussion

3.1. Flowing process in the retort

3.1.1. Flowing characteristics of gas

Figure 3 shows the flowing characteristics of gases and gaseous pyrolysis products. To ascertain the flowing characteristics of the main heat carrier (the reheated recycled gas), this paper firstly simulated its flowing process in the retort without regarding the generation of gaseous pyrolysis products and the flowing of the cold recycled gas. The reheated recycled gas flows firstly from the gas intake pipes into the annular channel, then into the in-core of the retort via the orifices in the wall of the retorting stage and support structures, and thereafter flows upward to heat the descending oil shale particles. Because of the resistance of the oil shale packing bed, the velocity of the reheated recycled gas is decreasing gradually during flowing to the three central parts of the retorting stage. This also shows that about 8.99% of the reheated recycled gas flows into the center pillar and then into the top half part of the retorting stage through the orifices connecting the center pillar and the retorting stage, to enhance the heating efficiency in the center part of the retort. Previously, the authors of the present paper had investigated the gas flow distribution in the retorting stage through a 1:5 scale three-dimensional cold physical model of the gas full circulation retort and found the distribution of the reheated recycled gas flow in the retorting stage to be maldistribution [30, 31]. The results of the mathematical model study obtained in this work were consistent with those of the physical model found by the authors earlier [30, 31].

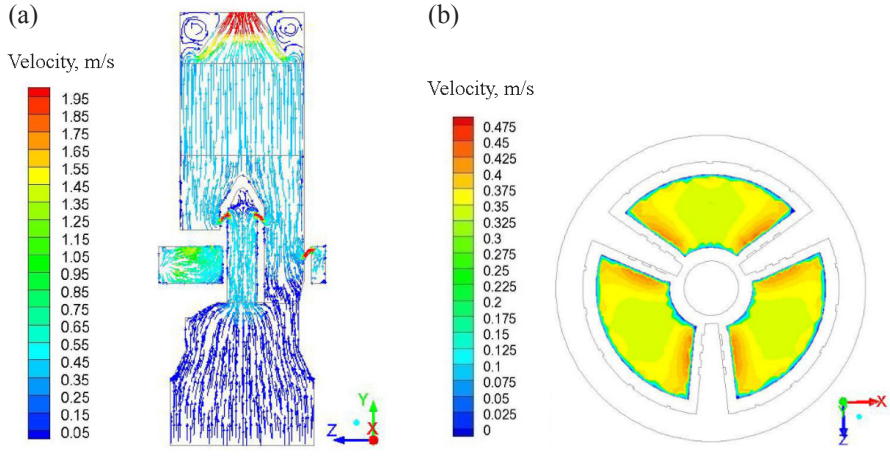

Fig. 3. The flowing traces ((a), X = 0 plane) and velocity contours ((b), Y = 5.37 m plane) of gases and gaseous pyrolysis products in the retort.

Then the pyrolysis reaction and the cold recycled gas flow were added in the mathematical model and the flow-thermo-pyrolysis process of the retorting process was investigated. In the retorting process, the cold recycled gas flows into the retort from the bottom of the cooling stage to make full use of the heat of spent shale, and is mixed with the reheated recycled gas at the bottom of the retorting stage. Part of the mixed recycled gas flows upside directly into the retorting stage. The other part of the mixed recycled gas (about 10.35%) flows into the center pillar and then into the top half part of the retorting stage through the orifices, which play an important role in heating the oil shale particles in the center part of the retort.

3.1.2. Flowing characteristics of oil shale particles

Figure 4 shows the flowing characteristics of oil shale/spent shale in the retort. During the downward-moving process, the flowing velocity of oil shale particles near the retort wall is smaller than that of the particles at the center of the retort on the same horizontal surface, and the velocity increases gradually from the wall toward the central region, due to the viscous force between the particles and the wall. Ying [32] simulated the axial and radial movement of particle materials using a physical Corex shaft furnace (model diameter 40 cm), and found that the particle velocity in the central region (radial 10–30 cm) of the shaft furnace was about 20 cm/h while the particle velocity near the side wall region (radial 0–10 cm and 30–40 cm) was linearly distributed at 2–20 cm/h, which was caused by the resistance of the furnace wall. Zhou et al. [33] and Zhang et al. [34] also found that the particles flow patterns in the shaft furnace showed an obvious profile evolution of 'Flat' to 'U' shape due to the friction between the particles and the wall in the downward-moving process.

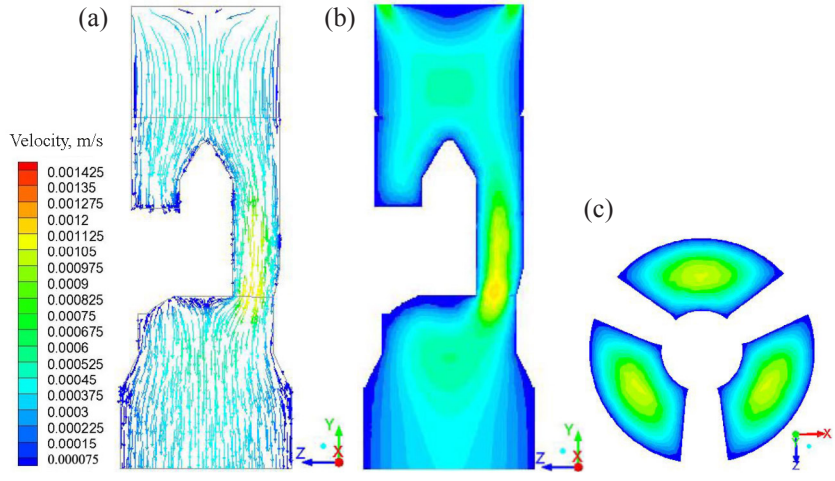

Fig. 4. The flowing traces ((a), X = 0 plane) and velocity contours ((b), X = 0 plane, (c), Y = 4.95 m plane) of oil shale/spent shale in the retort.

While the oil shale particles moving downward to the middle of the retorting stage at which the retort is divided into three parts by the center pillar and support structures, the particle velocity changes more significantly because the cross-section area is decreased by 27% compared to that of the pre-heating stage. Also, the oil shale particles can only move to the pre-heating stage from around the conical device which is used for collecting the oil-gas mixture, causing the particle velocity to be much smaller at the bottom of the device.

3.2. Heat transfer process in the retort

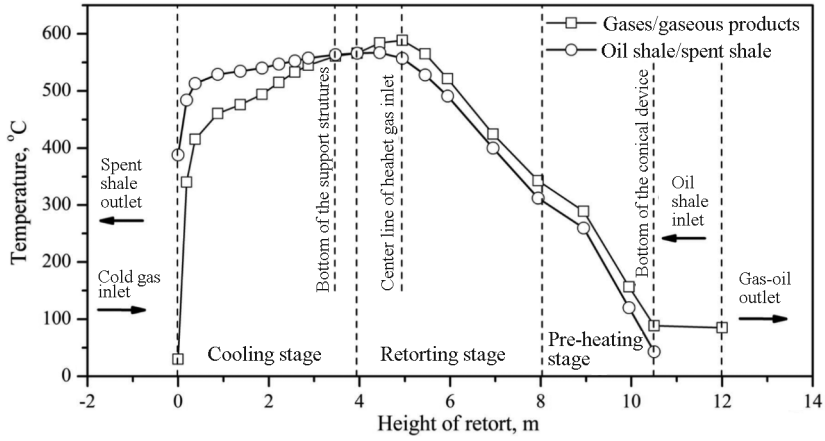

Fig. 5. The mass-weighted average temperature distribution of oil shale/spent shale and gases/gaseous products along the height of the retort.

Figure 5 shows the mass-weighted average temperature profile of oil shale/spent shale and gases/gaseous pyrolysis products along the height of the retort. Figures 6–8 display the temperature contours of oil shale/spent shale and gases/gaseous pyrolysis products in the retort. In the pre-heating and retorting stages, the temperature of gases is about 30 °C higher than that of oil shale on the same horizontal surface. Consequently, oil shale can be heated above 530 °C by the ascending high-temperature gases and pyrolyzed completely while moving downward to the bottom of the retorting stage. Meanwhile, the 640 °C reheated recycled gas, the gaseous pyrolysis products and the cold recycled gas having absorbed heat from spent shale are cooled down to about 85 °C and exhausted out from the conical device.

In the cooling stage, the broiling spent shale is cooled to 388 °C during moving down to the bottom of the stage by the cold recycled gas. Meanwhile, the heat exchange of the cold recycled gas with spent shale is basically stabilized as the gases ascend to the top of the cooling stage.

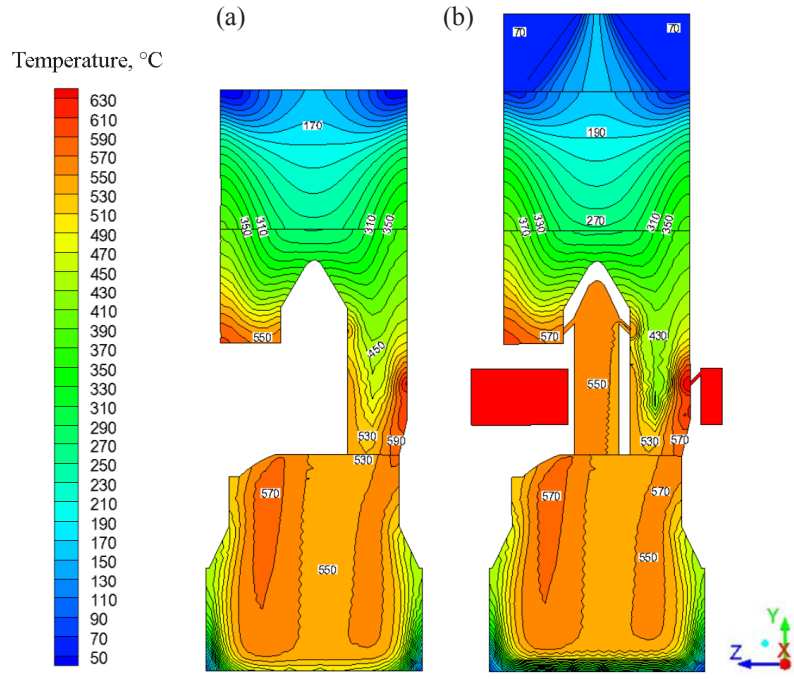

Fig. 6. The temperature contours of oil shale/spent shale (a) and gases/gaseous pyrolysis products (b) in the retort at X = 0 plane.

Figures 6–8 illustrate that the radial temperature distribution of the gases and oil shale/spent shale in the retort is uneven. The temperature of the gases and oil shale/spent shale decreases gradually from the retort wall regions to the central regions of the pre-heating and retorting stages. For example, the temperature of oil shale near the wall region exceeds 600 °C while the temperature of oil shale at the center of the three regions is about 475 °C at the height of 4.95 m (the height of the center line of the reheated recycled gas). This is mainly because of the non-uniform velocity distribution of the reheated recycled gas and oil shale, as described above. The flow rate of oil shale in the central regions is much higher and consequently, oil shale absorbs more heat, while on the contrary, both the velocity and temperature of the reheated recycled gas, which is the main heat carrier in the retort, gradually decrease through the heat transfer with oil shale particles during jetting from the orifices to the three central regions of the retorting stage. Similarly, the temperature of spent shale and the cold recycled gas increases gradually from the retort wall region to the central region in the cooling stage because the flow rate of the broiling spent shale is much higher in this stage.

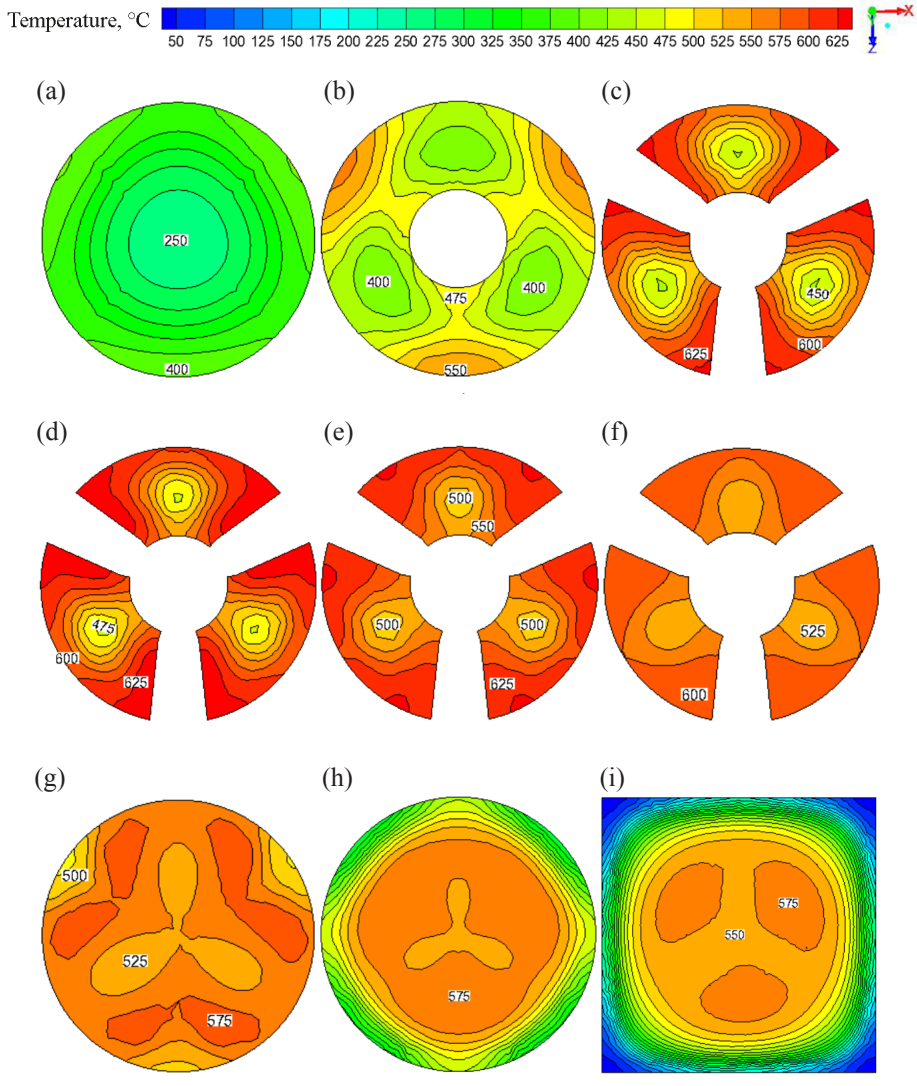

Fig. 7. The temperature contours of oil shale/spent shale at different heights of the retort: (a) 7.95 m; (b) 6.45 m; (c) 5.45 m; (d) 4.95 m; (e) 4.45 m; (f) 3.95 m; (g) 3.47 m; (h) 2 m; (i) 0.38 m.

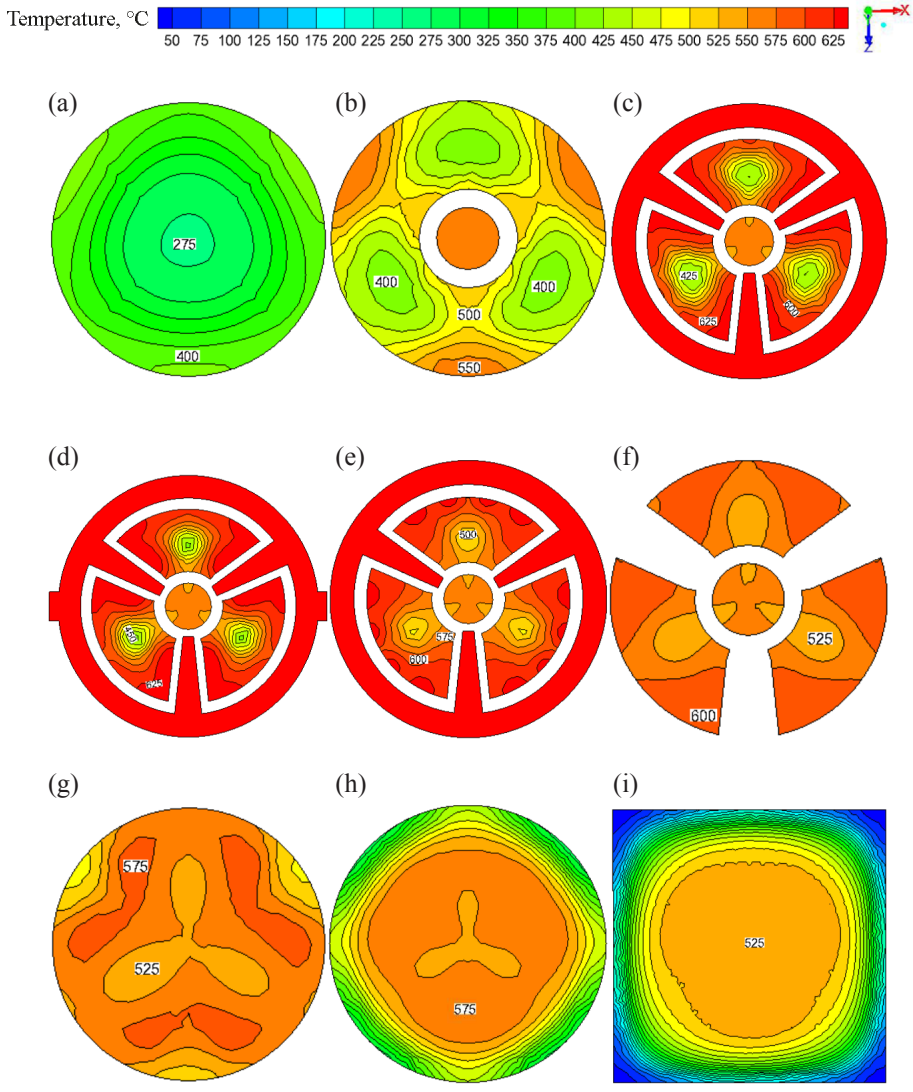

Fig. 8. The temperature contours of gases/gaseous pyrolysis products at different heights of the retort: (a) 7.95 m; (b) 6.45 m; (c) 5.45 m; (d) 4.95 m; (e) 4.45 m; (f) 3.95 m; (g) 3.47 m; (h) 2 m; (i) 0.38 m.

Figure 6 also illustrates that the temperature of gases is lower than that of oil shale in the three central regions of the retorting stage, which is mainly because the temperature of gaseous products generated actively from the shales in those regions is between 400 and 500 °C, which will reduce the mean temperature of gas after mixing it with the recycled gas.

3.3. Pyrolysis and mass transfer process in the retort

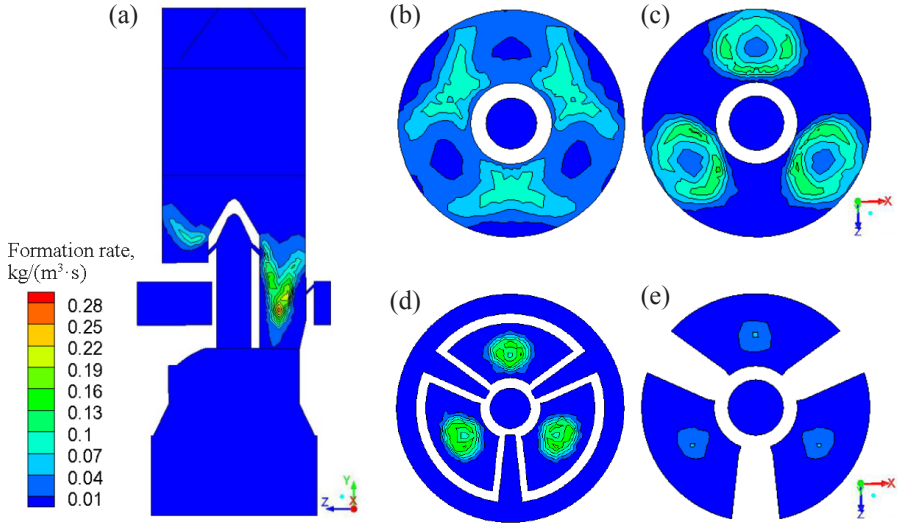

Fig. 9. The formation rate profile of gaseous pyrolysis products in the retort: (a) X = 0 plane; (b) Y = 6.47 m plane; (c) Y = 5.95 m plane; (d) Y = 5.45 m plane; (e) Y = 4.37 m plane.

The oil shale particles begin to convert into gaseous products and spent shale through the pyrolysis reaction as being heated to pyrolysis temperature. Figure 9 shows the formation rate profile of gaseous gas-oil-water products in the retort. The pyrolysis reaction of oil shale gradually diffuses from the wall (the wall of the retort, three support structures and the center pillar) regions to the central regions of the three retorting parts in the retorting stage during the downward-moving process because of the characteristic temperature distribution in the retort. The formation rate of gaseous products is much higher in the central regions of the three retorting parts because of the larger mass flow of oil shale particles in those regions.

As the oil shale particles move downward to the bottom of the retorting stage, kerogen in oil shale is pyrolyzed completely. The spent shales continue to move downward and will be discharged out of the retort ultimately by the discharging system. The gaseous products flow out with the recycled gases through the collection device situated at the top of the retort and then flow to the oil separation unit. The yield of gaseous products and spent shale recorded with the mathematical model is consistent with that obtained in aluminum retort experiments [28, 29].

3.4. Validation of the model

Based on the series of theoretical and simulation analyses performed by the authors previously [30, 31] and in the current paper, 64 gas full circulation oil shale retorts have been constructed in the Shichanggou oil shale retorting plant in Jimsar oil shale mineralized belt, Xinjiang Uygur Autonomous Region, northwestern China. To validate the heat transfer process of the mathematical model in this paper, the real temperature of gases at the outlet pipe was measured in 16 retorts and the design temperature of spent shale at the bottom of the cooling stage was theoretically calculated according to the conservation of mass and energy, as shown in Table 2. The oil shale particle group used in the above numerical simulation consisted of 60% of 20–50 mm, 17% of 50–55 mm, 20% of 6–20 mm and 3% of 0–6 mm oil shale particles, which is consistent with the actual production situation within a required timeframe. It is clear that the numerical results are in good agreement with the data obtained in the real retort, with the relative error less than 5.29%.

Table 2. The temperature of gas and spent shale at different outlets of the retort

	Numerical data	Measured data	Design data	Relative error
Temperature of gas at the outlet pipe, °C	85.24	80–100	90–110	5.29%
Temperature of spent shale at the outlet of the cooling stage, °C	388.26	–	370	4.93%

3.5. The influence of oil shale particle size on the retorting process

In this work, the influence of oil shale particle size (6–20, 20–30, 30–50, 50–55 mm) on the retorting process is determined. Figures 10a and 10b show the mass-weighted average temperature distribution along the height of the retort while retorting four oil shale particle groups of different size ranges at the same treatment capacity (300 t/d) and the same reheated recycled gas consumption. With increasing particle size, the final retorting temperature of oil shale is decreased from 584 °C to 544 °C, the outlet temperature of gaseous products is increased from 77 °C to 96 °C, the yield of spent shale is increased from 86.27% to 87.92% and the yield of gaseous products is decreased from 13.73% to 12.08%. These results reveal that oil shale particles in the size range of 30–50 and 50–55 mm were not pyrolyzed completely at the treatment capacity of 300 t/d.

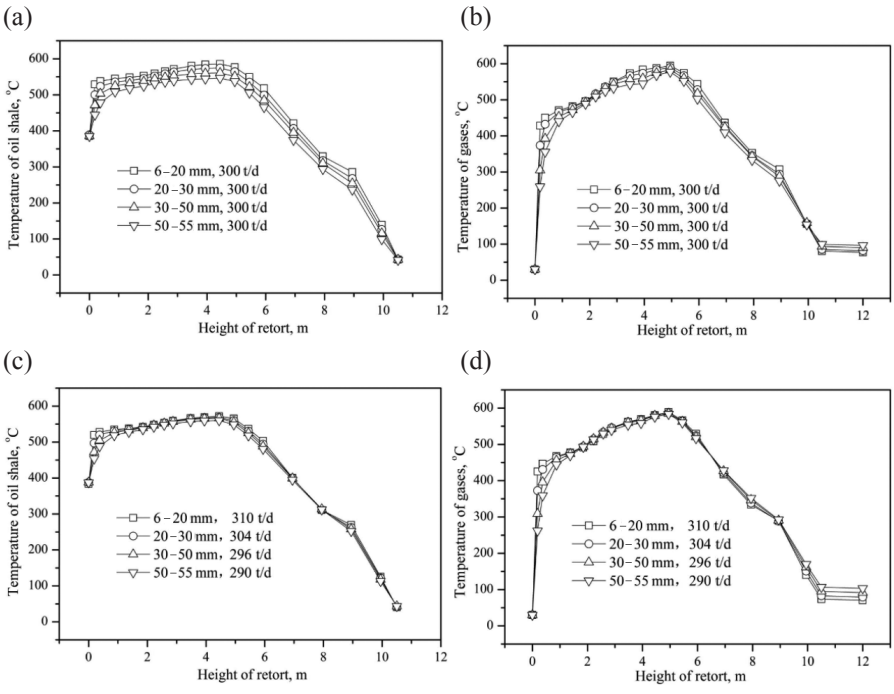

Fig. 10. The temperature distribution of oil shale/spent shale ((a), (c)) and gas/gaseous pyrolysis products ((b), (d)) along the height of the retort while retorting oil shale in different particle size ranges at different treatment capacities and the same reheated gas consumption.

According to Equations (6)–(8), the volumetric convection heat transfer coefficient between oil shale and the gaseous heat carrier is decreased with increasing oil shale particle size, which results in that the heat transfer capacity is insufficient to pyrolyze the 30–50 and 50–55 mm oil shale particle groups. The oil shale processing capacity should gradually decrease with increasing particle size. Through the numerical simulation, the optimal processing capacity of oil shale of different particle size ranges is shown in Figures 10c and 10d, as the reheated recycled gas consumption remains unchanged.

What's more, the excessive capacity of heat transfer between 6–20 mm oil shale particles and the gaseous heat carrier results in that the temperature around the walls in the retorting stage significantly exceeds the optimal retorting temperature, which will cause the pyrogenic reaction of shale oil and the broken spent shale. Hence, oil shale particles larger than 50 mm and smaller than 20 mm should be mixed with 20–50 mm particles at a proper ratio rather than feeding them into the retort directly, to increase oil yield and enhance the thermal efficiency and processing capacity of the retort.

The oil shale particle size also has an obvious effect on the pressure of the annular gas channel. The reheated recycled gas pressure in the annular gas channel is 4780, 850, 465 and 240 Pa, respectively, as the particle size of retorted oil shale groups increases from 6–20 mm to 50–55 mm. With decreasing particle size, the voidage of the oil shale packing bed is decreased and its resistance is increased [26], which results in the increase of the pressure in the annular gas channel and the load of blowers. From the perspective of decreasing the loss of oil in the pre-heating stage and the load of the reheated gas transport system, the 6–20 mm oil shale particles should be mixed with 20–50 mm particles at a proper ratio, or be pelletized with 0–6 mm oil shale powder by using pelletizers.

4. Conclusions

In this work, a 3-D mathematical model is developed to investigate the flow distribution, temperature distribution and evolution of gaseous pyrolysis products in the 300 t/d gas full circulation oil shale retort. The simulated results are coincident with findings obtained in cold model experiments, as well as with operation data. The main conclusions are as follows:

(1) The velocity of reheated recycled gas decreases gradually during flowing from the orifices to the three central parts of the retorting stage. About 10.35% of the total recycled gas can flow into the top half part of the retorting stage through the center pillar and play an important role in heating the oil shale particles in the central part of the retort.

(2) The velocity of oil shale particles increases gradually from the wall regions toward the central regions of the retort on the same horizontal surface, due to the viscous force between the particles and the wall.

(3) In the pre-heating and retorting stages, the average temperature of gases is about 30 °C higher than that of oil shale on the same level, and the temperature of gases and oil shale/spent shale decreases gradually from the retort wall regions to the central regions.

(4) Oil shale particles larger than 50 mm and smaller than 20 mm should be mixed with 20–50 mm oil shale particles at a proper ratio rather than feeding them into the retort directly, to increase oil yield and enhance the thermal efficiency and processing capacity of the retort.

Acknowledgements

Project 51904209 supported by National Natural Science Foundation of China.

REFERENCES

1. Mozaffari, P., Baird, Z. S., Listak, M., Oja, V. Vapor pressures of narrow gasoline fractions of oil from industrial retorting of Kukersite oil shale. *Oil Shale*, 2020, **37**(4), 288–303.
2. Sabanov, S., Mukhamedyarova, Z. Prospectivity analysis of oil shales in Kazakhstan. *Oil Shale*, 2020, **37**(4), 269–280.
3. Dong, R. T., Xia, L. Z., Wang, H. N., Jiao, D. S. 3-D CFD simulation of oil shale drying in fluidized bed and experimental verification. *Oil Shale*, 2020, **37**(4), 334–356.
4. Bai, J. R., Bai, Z., Wang, Q., Li, S. Y. Process simulation of oil shale comprehensive utilization system based on Huadian-type retorting technique. *Oil Shale*, 2015, **32**(1), 66–81.
5. Yue, C. T., Liu, Y., Ma, Y., Li, S. Y., He, J. L., Qiu, D. K. Influence of retorting conditions on the pyrolysis of Yaojie oil shale. *Oil Shale*, 2014, **31**(1), 66–78.
6. Qian, J. L., Yin, L., Wang, J. Q., Li, S.Y., Han, F., He, Y. G. *Oil Shale – Petroleum Alternative*. China Petrochemical Press, Beijing, 2010.
7. Lin, L. X., Zhang, C., Li, H. J., Lai, D. G., Xu, G. W. Pyrolysis in indirectly heated fixed bed with internals: The first application to oil shale. *Fuel Process. Technol.*, 2015, **138**, 147–155.
8. Wang, Q. Q., Ma, Y., Li, S. Y., Yue, C. T., He, L. Expanding exergy analysis for the sustainability assessment of SJ-type oil shale retorting process. *Energ. Convers. Manag.*, 2019, **187**, 29–40.
9. He, J. L., Wang, Q. Development and application of Estonia Galoter technology. *Journal of Northeast Dianli University*, 2016, **36**(2), 76–80 (in Chinese).
10. Wu, Q. C. *Oil Shale Dry Distillation Technology*. Liaoning Science and Technology Publishing House, Shenyang, 2012 (in Chinese).
11. Stahnke, C., Silva, M. K., Rosa, L. M., Noriler, D., Martignoni, W. P., Bastos, J. C. S. C., Meier, H. F. Oil shale reactor: process analysis and design by CFD. *Chem. Eng. Res. Des.*, 2019, **152**, 180–192.
12. Rebordinos, J. G., Herce, C., Gonzalez-Espinosa, A., Gil, M., Cortes, C., Brunet, F., Ferre, L., Arias, A. Evaluation of retrofitting of an industrial steam cracking furnace by means of CFD simulations. *Appl. Therm. Eng.*, 2019, **162**, 114206.
13. Peng, J., Chen, D. Q., Xu, J. J., Hu, L., Liu, H. Z. CFD simulation focusing on void distribution of subcooled flow boiling in circular tube under rolling condition. *Int. J. Heat Mass Tran.*, 2020, **156**, 119790.
14. Zhou, H. R., Zeng, S., Yang, S. Y., Xu, G. W., Qian, Y. Modeling and analysis of oil shale refinery process with the indirectly heated moving bed. *Carbon Resour. Convers.*, 2018, **1**(3), 260–265.
15. Wang, Q., Wang, Y. F., Zhang, H. X., Xu, X. C., Yang, Q. K., Wang, P. The simulation study of application of the FG-DVC model to the pyrolysis of Huadian oil shale of China at different heating rates. *Oil Shale*, 2016, **33**(2), 111–124.
16. You, Y. L., Wang, X. Y., Han, X. X., Jiang, X. M. Kerogen pyrolysis model

based on its chemical structure for predicting product evolution. *Fuel*, 2019, **246**, 149–159.
17. Fletcher, T. H., Barfuss, D., Pugmire, R. J. Modeling light gas and tar yields from pyrolysis of Green River oil shale demineralized kerogen using the chemical percolation devolatilization model. *Energy Fuels*, 2015, **29**(8), 4921–4926.
18. Wang, Q., Ren, L. G., Wang, R., Bai, J. R., Wang, H. T., Yan, Y. H. Characterization of oil shales by ^{13}C-NMR and the simulation of pyrolysis by FLASHCHAIN. *J. Fuel Chem. Technol.*, 2014, **42**(3), 303–308 (in Chinese).
19. Lin, W., Feng, Y. H., Zhang, X. X. Numerical study of volatiles production, fluid flow and heat transfer in coke ovens. *Appl. Therm. Eng.*, 2015, **81**, 353–358.
20. Jin, K., Feng, Y. H., Zhang, X. X., Wang, M. D., Yang, J. F., Ma, X. B. Simulation of transport phenomena in coke oven with staging combustion. *Appl. Therm. Eng.*, 2013, **58**(1–2), 354–362.
21. Modest, M. F. *Radiative Heat Transfer*, 2nd Edition. Academic Press, San Diego, 2003.
22. Wang, F. Q., Tan, J. Y., Yong, S., Tan, H. P., Chu, S. X. Thermal performance analyses of porous media solar receiver with different irradiative transfer models. *Int. J. Heat Mass Tran.*, 2014, **78**, 7–16.
23. Chen, X., Sun, C., Xia, X. L., Liu, R. Q., Wang, F. Q. Conjugated heat transfer analysis of a foam filled double-pipe heat exchanger for high-temperature application. *Int. J. Heat Mass Tran.*, 2019, **134**, 1003–1013.
24. Wang, F. Q., Shuai, Y., Wang, Z. Q., Leng, Y., Tan, H. P. Thermal and chemical reaction performance analyses of steam methane reforming in porous media solar thermochemical reactor. *Int. J. Hydrog. Energy*, 2014, **39**(2), 718–730.
25. Wang, F. Q., Yong, S., Tan, H. P., Yu, C. L. Thermal performance analysis of porous media receiver with concentrated solar irradiation. *Int. J. Heat Mass Tran.*, 2013, **62**, 247–254.
26. Pan, L.W., Dai, F. Q., Tian, Y. Q., Zhang, F. H. Experimental investigation of the sphericity of irregularly shaped oil shale particle groups. *Adv. Powder Technol.*, 2015, **26**(1), 66–72.
27. Guo, Z. C., Tang, H. Q. Numerical simulation for a process analysis of a coke oven. *China Particuology*, 2005, **3**(6), 373–378.
28. Pan, L. W., Dai, F. Q., Li, G. Q., Liu, S. A TGA/DTA-MS investigation to the influence of process conditions on the pyrolysis of Jimsar oil shale. *Energy*, 2015, **86**, 749–757.
29. Pan, L. W., Dai, F. Q., Huang, J. N., Liu, S., Li, G. Q. Study of the effect of mineral matters on the thermal decomposition of Jimsar oil shale using TG-MS. *Thermochim. Acta*, 2016, **627–629**, 31–38.
30. Pan, L. W., Dai, F. Q., Huang, J. N., Liu, S., Zhang, F. H. Investigation of the gas flow distribution and pressure drop in Xinjiang oil shale retort. *Oil Shale*, 2015, **32**(2), 172–185.
31. Pan, L. W., Dai, F. Q., Huang, J. N., Liu, S., Zhang, F. H. Study of a new gas inlet structure designed for Xinjiang oil shale retort. *Oil Shale*, 2016, **33**(1), 69–79.

32. Ying, W. F. *Mathematical & Physical Simulation of COREX Pre-Reduction Shaft Furnace*. Northeastern University, Shengyang, 2013 (in Chinese).
33. Zhou, H., Zou, Z. S., Luo, Z. G., Zhang, T., You, Y., Li, H. F. Analyses of solid flow in latest design COREX shaft furnace by physical simulation. *Ironmak. Steelmak.*, 2015, **42**(3), 209–216.
34. Zhang, X. S., Zou, Z. S., Luo, Z. G. Influence of CGD structure on burden descending behavior in COREX shaft furnace. *Metall. Res. Technol.*, 2019, **116**(3), 304.